

Quantitative Analysis of Electronic Properties of Carbon Nanotubes by Scanning Probe Microscopy: From Atomic to Mesoscopic Length Scales

Vincent Meunier,¹ Sergei V. Kalinin,² Junsoo Shin,^{2,3} Arthur P. Baddorf,² and Robert J. Harrison¹

¹Computer Science and Mathematics Division, Oak Ridge National Laboratory, Oak Ridge, Tennessee 37831, USA

²Condensed Matter Sciences Division, Oak Ridge National Laboratory, Oak Ridge, Tennessee 37831, USA

³Department of Physics and Astronomy, University of Tennessee, Knoxville, Tennessee 37996, USA

(Received 24 May 2004; published 6 December 2004)

A new multiscale approach to the quantitative interpretation of scanning probe microscopy data in terms of the local electronic properties of 1D systems such as carbon nanotubes is presented. The interactions between a probe and the system are treated using a combination of first-principles density functional calculations and continuum electrostatics modeling. Realistic tip size effects are included using an image charge model. It is shown that the local potential at a nanotube on a substrate due to a probe can be calculated quantitatively, allowing experimental data to be analyzed in terms of the electronic structure of defects.

DOI: 10.1103/PhysRevLett.93.246801

PACS numbers: 73.22.-f, 61.46.+w, 68.37.-d, 71.15.-m

Local transport imaging techniques such as scanning gate microscopy (SGM)[1] and scanning impedance microscopy (SIM)[2] provide great power for understanding the transport properties of 1D systems such as carbon nanotubes and semiconductor nanowires. SGM images the change in the local resistance due to the presence of a field generated by a probe (field-effect imaging) [3,4], while SIM measures the local potential amplitude in an operational nanocircuit [4]. Recently, a combination of low temperature scanning probe microscopies (SPMs) was used to study the defect mediated charge dynamics in carbon nanotube circuits, providing real-space images of quantum interference patterns in 1D structures [5,6]. Despite this outstanding progress, transport SPMs have largely been qualitative techniques since the complexity of the electrostatic probe-sample interactions and the geometry of the system have precluded rigorous interpretation of SPM data in terms of atomic-scale properties [7].

In this Letter, we present a systematic approach for a quantitative analysis of the SPM measurements on carbon nanotubes that can readily be extended to other 1D systems, such as semiconductor nanowires. While the screening of nanotubes in the presence of a uniform field was addressed previously [8–10], here we combine different levels of theory to analyze the screening in a nanotube in the presence of a strongly *nonuniform* localized field required to attain high spatial resolution in SPM. To achieve this, large scale first-principles modeling of the interactions between a point charge and a carbon nanotube is combined, for the first time, with continuum theory (CT) to encompass effects ranging from atomic to mesoscopic length scales. This multiscale modeling is extended to a realistic tip geometry, ultimately yielding a robust description of the tip-sample interactions at all length scales (0.5–200 nm) used in modern SPM measurements.

All-electron density functional theory (DFT) (local density approximation) calculations of conducting single

wall nanotubes (SWNTs) were performed using NWChem [11] in the 6-31g* (Ref. [12]) atom-centered, contracted Gaussian basis sets, using the DGAUSS A1 [13] set for variational fitting [14] of the Coulomb potential during calculation of the self-consistent solution. Once converged, the total potential (electronic and nuclear) was computed *without* charge fitting. The 6-31g* basis includes functions on each site for radial (*s* and *p*) and angular polarization (*p* and *d*). Calculations of the polarizability of small molecules with free-space boundary conditions often employ higher (*f*, etc.) polarization functions and also additional diffuse functions. For large systems, such as the ones studied here, it is not computationally feasible to include more functions, and diffuse functions on each site would lead to catastrophic numerical linear dependence. However, in contrast to small molecules, the response of the nanotube (which would be a conductor if infinitely long) to the strong external field is neither primarily on site nor due to the long tail of the density, but arises from the redistribution of charge between sites. Thus, the 6-31g* basis is expected to yield an accurate electrostatic potential external to the molecular charge distribution [15].

The DFT calculations yield a spatially resolved electrostatic potential distribution, V_a , in the point charge-nanotube system and include charge screening and electron redistribution effects (Fig. 1). As a “molecule-in-a-box” calculation, the potential corresponds to a *floating* neutral system that differs from a *grounded* one in that the total charge on the nanotube remains constant. In actual experiments the one-dimensional system is contacted to the macroscopic world by electrodes and charge flows from the external circuit to equalize the electrochemical potential throughout the system. To address this difference in electrostatic boundary conditions, we have additionally calculated the potential distribution, V_b , in the point charge-nanotube system with additional charge (typically one electron) placed on the nanotube. The

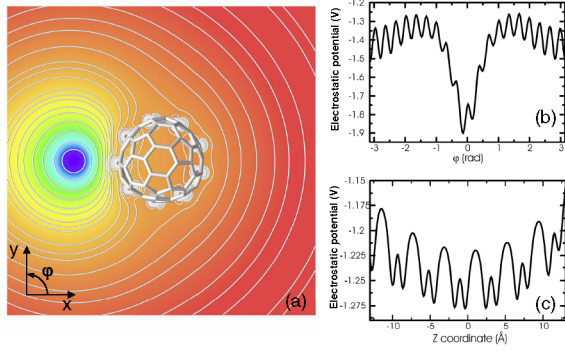


FIG. 1 (color online). Electrostatic potential distribution induced by a point charge located 7 \AA from a $(9, 0)$ capped carbon nanotube. (a) Potential on a plane perpendicular to the tube. (b) Potential around the effective tube circumference, 0.7 \AA outside of the tube sidewall. (c) Potential along the tube, 2 \AA from the sidewall.

difference in potentials, $V_d = V_b - V_a$, describes the behavior of a free charge on the finite SWNTs in the presence of external charge. It is illustrated in Fig. 2(a) for various tube lengths.

The external charge induces a polarization on the nanotube which decays slowly along the tube, in agreement with electrostatics of one-dimensional systems [16]. The uniformity of the potential inside the nanotube and the symmetry, with respect to the tube axis, suggest that the charge dynamics of the point charge deposited on the nanotube can be well described by a continuum model for a hollow charged cylinder. For an infinite charged cylinder, the potential distribution is given by $V_{c0}(r) = \lambda/2\pi\epsilon_0 \ln(a_2/a_1)$ inside and $V_c(r) = \lambda/2\pi\epsilon_0 \times \ln(a_2/r)$ outside the cylinder, where a_1 is the effective electrostatic radius of the nanotube, λ is the charge den-

sity, and a_2 is the external cutoff radius related to the nanotube length.

For all nanotubes longer than 11 \AA [Fig. 2(b)], the effective electrostatic radius matching the DFT calculations is 4.1 \AA , as compared to the geometrical radius of 3.4 \AA , a signature of the fact that the excess charge resides on the outward lobes of the π^* orbitals, which on average extend 0.7 \AA outside the atomic centers [8]. The external cutoff radius scales linearly with the number of atoms (not shown), as expected for a finite cylinder. Shown in Fig. 2(c) is the potential at the center of the nanotube compared with the approximate expression for the finite conductive cylinder of length L with charge q , $V_0(L) = \lambda/2\pi\epsilon_0 \ln(L/a_1) = q/(2\pi\epsilon_0 L) \ln(L/a_1)$. The excellent agreement between continuum electrostatics and DFT, despite the lack of free parameters, shows that the free charge dynamics on a finite metallic carbon nanotube is well described using a conductive cylinder model, $V_d \sim V_c$, independent of external charge conditions. Thus, the potential distribution in the floating and grounded systems can be related as $V_a = V_g + \alpha V_c$, where α is a coefficient that accounts for the magnitude of the induced charge on the nanotube. The correspondence between DFT and CT descriptions can be established by imposing that the DFT and CT results coincide at the nanotube boundary. The electric field, $E = dV/dx|_{x=0}$, at the center of the nanotube, provides the measure of deviation from an ideal conductive cylinder behavior due to the finite density of states on the nanotube. This behavior does not depend on the nanotube length, as illustrated in Fig. 2(d). Note that while the potential on the nanotube decreases as a function of its length, the electrostatic field at the center remains constant.

Since our DFT calculations are practically limited to finite tube lengths and small tube-charge distances, it is imperative to construct a continuum electrostatic model to extend the *ab initio* theory [17]. Any description of the interaction between a point charge and a one-dimensional system must account for the finite density of states of the latter [9,18]. In our extension to continuum electrostatics, the quantum contribution to the electrostatic properties is described using the inverse screening length, k_s , which relates the surface charge density and the surface potential as $\sigma_s = k_s \epsilon_0 V_s$. In cylindrical coordinates where the z axis coincides with the tube axis, the point charge is located at distance ρ in the $\varphi = 0$ direction at $z = 0$. The potential distributions inside the nanotube, $V_n(r, \rho, \varphi, z)$, and in vacuum, $V_v(r, \rho, \varphi, z)$, for $r < \rho$ are then given by

$$V_n = \sum_{m=-\infty}^{\infty} \int_0^{\infty} dk \cos(kz) e^{im\varphi} A_{mk} I_m(kr),$$

$$V_v = \sum_{m=-\infty}^{\infty} \int_0^{\infty} dk \cos(kz) e^{im\varphi} [B_{mk} I_m(kr) + C_{mk} K_m(kr)],$$
(1)

where I_m and K_m are Bessel functions of the second kind,

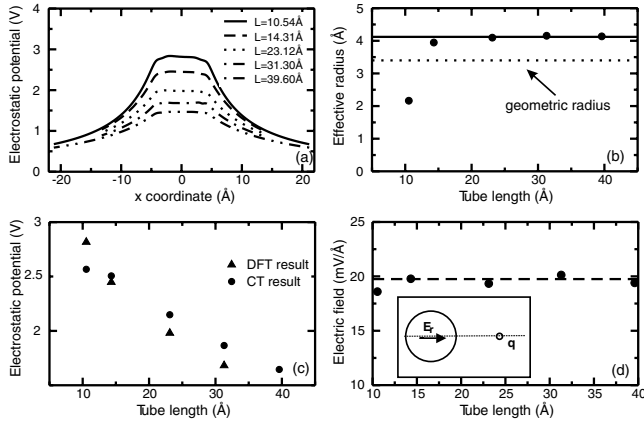


FIG. 2. (a) Effective potential, V_d , of a $(9, 0)$ charged nanotube along the perpendicular direction for different nanotube lengths. (b) Effective electrostatic radius, which converges quickly to a constant value, for tube lengths larger than about 3 to 4 times the radius. (c) Potential at the center of the nanotube from the DFT calculations and the electrostatic approximation as a function of nanotube length and (d) corresponding DFT electric field.

A_{mk} and C_{mk} are coefficients determined by boundary conditions [19], and B_{mk} comes from the bare potential of the charge. The boundary conditions, at $r = R$, for a dielectric cylinder (of radius R) with finite surface density of states reflect the continuity of the potential and the linear screening approximation, respectively:

$$V_n = V_v, \quad \text{and} \quad \epsilon \frac{dV_n}{dr} - \frac{dV_v}{dr} = -k_s V_s, \quad (2)$$

where ϵ is the bulk dielectric constant. The potentials in vacuum and inside the nanotube are obtained from Eqs. (1) and (2):

$$\begin{aligned} B_{mk} &= \frac{q}{2\pi^2 \epsilon_0} K_m(k\rho), \\ A_{mk} &= B_{mk} \frac{I'_m(kR)K_m(kR) - I_m(kR)K'_m(kR)}{D_{mk}}, \\ C_{mk} &= -B_{mk} I_m(kR) \frac{k_s I_m(kR)/k + (\epsilon - 1)I'_m(kR)}{D_{mk}}, \end{aligned} \quad (3)$$

where $D_{mk} = \epsilon I'_m(kR)K_m(kR) + I_m(kR)[k_s K_m(kR)/k - K'_m(kR)]$ [20]. The above approximation is *a priori*, applicable only to infinite 2D systems. This is not exactly the case for a SWNT where the energy is quantized around its circumference. A more rigorous solution would include distinct longitudinal and circumferential screening lengths. We address this issue by considering k_s as an effective parameter that depends on the charge-tube separation [Fig. 3(a)]. Practically, the effective k_s value for different charge-tube separations is determined so that the electric field at the center of the tube matches that of the DFT calculation. We find that the distance dependence can be approximated by $k_s(x) = k_{si} + b/x$, where $k_{si} = 5.0 \pm 0.1 \text{ \AA}^{-1}$ and $b = 12.4 \pm 0.3$. The distance dependence originates from the fact that the electrostatic screening becomes less effective when the charge is moved away from the tube, since for a small charge-tube distance there is a large tangential component of the field which induces longitudinal polarization in the sp^2 bonded electron system of the nanotube. For large charge-tube separations, the field is essentially normal to the surface, and the screening is dominated by the p_z orbitals.

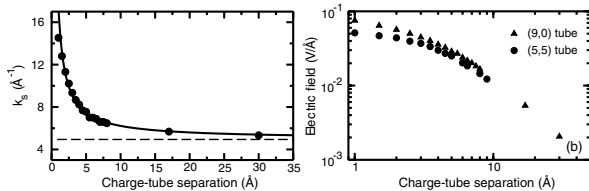


FIG. 3. (a) Effective screening length for a (9, 0) nanotube as a function of the charge-tube separation. (b) Electric field at the center of the (5, 5) and (9, 0) nanotubes as a function of charge-tube separation, as computed by DFT.

To demonstrate the universality of the model, we have computed the charge-tube separation dependence of the electrostatic field at the center of (5, 5) and (9, 0) nanotubes [Fig. 3(b)]. There is a significant difference in the electrostatic behavior of the nanotubes for small charge surface separations, which is the expression of the different atomic structures and, in turn, of the atomic mechanism of screening. At large charge-tube separations, the screening behaviors become virtually identical. To account for the difference in biasing conditions, the potential of the nanotube in CT is corrected as $V_{\text{eff}} = V_g + \alpha V_c$, with $\alpha = 0.56$ being the induced charge on the nanotube per electron present on the tip. With this correction, the potential distributions in the DFT and CT models are very similar, the main difference remaining at the locations of the atoms due to the atomic polarizabilities [Fig. 4(a)].

We now use the DFT-based continuum electrostatic model to describe the electrostatic interactions between a spherical SPM tip and a nanotube on a flat substrate. Under typical SGM experimental conditions, the tip radius of curvature and the tip-substrate separation (ranging from 10 to 100 nm and 3 to 500 nm, respectively) are significantly larger than the typical 0.5–3 nm radius of a nanotube. This implies that the nanotube-tip capacitance is negligible compared to the tip-substrate capacitance and the charge states of the tip are only weakly affected by the nanotube. Thus, the point charge interaction can be extended to the spherical tip model as follows: In the sphere-plane approximation, the image charge distribution in the tip can be represented by a set of charges Q_i located at distances r_i from the center of the sphere such that

$$Q_{i+1} = \frac{\kappa - 1}{\kappa + 1} \frac{r_{i+1}}{R_{\text{tip}}} Q_i, \quad r_{i+1} = \frac{R_{\text{tip}}^2}{2(R_{\text{tip}} + d) - r_i}, \quad (4)$$

where R_{tip} is the tip radius, κ is the dielectric constant of the substrate, d is the tip-surface separation, $Q_0 = 4\pi\epsilon_0 \times R_{\text{tip}} V$, $r_0 = 0$, and V is the tip bias. Hence, the tip induced potential on the nanotube is, with $\rho_0^i = R_{\text{tip}} + d - r_i$,

$$V_t = \sum_{i=0}^{\infty} \left[Q_i v_s(\rho_0^i - 2R) - \frac{\kappa - 1}{\kappa + 1} Q_i v_s(\rho_0^i + 2R) \right], \quad (5)$$

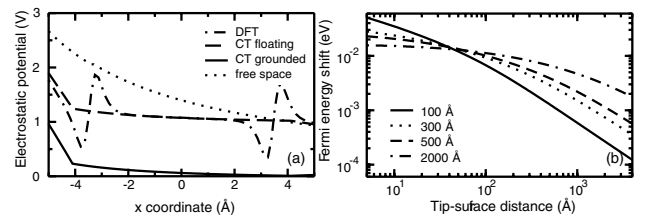


FIG. 4. (a) Electrostatic potential perpendicular to the nanotube from the DFT model, compared to the electrostatic model for grounded and floating nanotubes. (b) Fermi energy shift in the nanotube as a function of tip-surface separation for $V_{\text{tip}} = 1 \text{ V}$.

where the first term is due to the image charges in the tip and the second term comes from the image charges in the substrate. The potential induced by one electron, $v_s(\rho)$, is a rapidly decaying function of tip-surface separation (faster than $1/\rho$), and, for large tip-tube separations, $d \gg R_{\text{tip}}$, Eq. (5) is simplified to $V_t = 2v_s(R_{\text{tip}} + d)CV/(\kappa + 1)$, where C is the tip-surface capacitance that depends only on geometry, for a dielectric substrate. Note that for a metallic substrate the potential is approximately given by $V_t = 4RCV\partial v_s(R_{\text{tip}} + d)/\partial z$. Given that different limiting behaviors are expected for large separations and large dielectric constants, the use of Eqs. (4) and (5) is required for quantitative evaluations.

We can now analyze the distance dependence of the Fermi energy shift in the nanotube corresponding to a given bias applied to the tip [Fig. 4(b)]. The potential on the nanotube is only a fraction (10^{-3} to 10^{-2}) of the applied tip bias. Thus, the application of ~ 10 V to the SPM tip shifts the Fermi level on the nanotube by tens of meV, comparable with the estimated energy levels of defects. It has long been realized that the shift of the Fermi level of the nanotube is significantly smaller than the tip bias. Notably, Woodside [5] has used a simple electrostatic model to describe the decay of electrostatic potential at large separation from the tip. A similar approach taking into account quantum capacitance of the nanotube was employed by Freitag *et al.* [7] to describe experimental SGM data on semiconductive nanotubes. However, both these approaches are phenomenological and do not explicitly address the electrostatics of tip, tube, and substrate interactions as developed here. Furthermore, comparison between the present rigorous theory and the approximate result indicates that the difference in the Fermi level shift does not exceed a factor of ~ 5 , significantly less than the 2–3 order of magnitude difference between tip bias and Fermi level shift.

In summary, we have shown that the combination of first-principles and continuum theory applied to the analysis of the interaction between a probe and a one-dimensional system on a substrate leads to a straightforward numerical interpretation of the SPM data in terms of relevant electronic properties of the system which ultimately lead to a full description of defects. Only such a rigorous analysis of tip-surface interactions taking into account quantum capacitance of the system and localized properties of the tip allows one to quantitatively relate tip bias and Fermi level on reduce-dimensionality systems unambiguously. The only unknown parameter is the tip radius of curvature, which can be determined from the SIM measurements as reported elsewhere [21].

This research is supported by the Division of Materials Science, and R.J.H. acknowledges support from the Mathematics, Information, and Computing Division, U.S. Department of Energy under Contract No. DE-AC05-00OR22725 with UT-Battelle, LLC at Oak Ridge National Laboratory.

- [1] M. A. Eriksson, R. G. Beck, M. Topinka, J. A. Katine, R. M. Westervelt, K. L. Campman, and A. C. Gossard, *Appl. Phys. Lett.* **69**, 671 (1996).
- [2] S.V. Kalinin and D. A. Bonnell, *Appl. Phys. Lett.* **78**, 1306 (2001).
- [3] S. J. Tans and C. Dekker, *Nature (London)* **404**, 834 (2000).
- [4] A. Bachtold, M. S. Fuhrer, S. Plyasunov, M. Forero, E. H. Anderson, A. Zettl, and P. L. McEuen, *Phys. Rev. Lett.* **84**, 6082 (2000).
- [5] M. T. Woodside, Ph.D. thesis, University of California, Berkeley, 2001.
- [6] M. T. Woodside and P. L. McEuen, *Science* **296**, 1098 (2002).
- [7] M. Freitag, A. T. Johnson, S. V. Kalinin, and D. A. Bonnell, *Phys. Rev. Lett.* **89**, 216801 (2002).
- [8] L. X. Benedict, S. G. Louie, and M. L. Cohen, *Phys. Rev. B* **52**, 8541 (1995).
- [9] M. R. Krcmar and W. M. Saslow, *Phys. Rev. B* **66**, 235310 (2002); M. R. Krcmar, W. M. Saslow, and A. Zangwill, *J. Appl. Phys.* **93**, 3495 (2003).
- [10] S. V. Rotkin and K. Hess, *Appl. Phys. Lett.* **84**, 3139 (2004); Y. Li, S. V. Rotkin, and U. Ravaioli, *Nano Lett.* **3**, 183 (2003).
- [11] High Performance Computational Chemistry Group, computer code NWChem, a computational chemistry package for parallel computers, version 4.5, Pacific Northwest National Laboratory, Richland, Washington 99352, USA, 2003; R. A. Kendall *et al.*, *Comput. Phys. Commun.* **128**, 260 (2000).
- [12] J. Hehre, R. Ditchfield, and J. A. Pople, *J. Chem. Phys.* **56**, 2257 (1972).
- [13] N. Godbout, D. R. Salahub, J. Andzelm, and E. Wimmer, *Can. J. Chem.* **70**, 560 (1992).
- [14] B. I. Dunlap, J. W. D. Connolly, and J. R. Sabin, *J. Chem. Phys.* **71**, 3396 (1979).
- [15] To quantify this, we also used the smaller 3-21g basis [J. S. Binkley, J. A. Pople, and W. J. Hehre, *J. Am. Chem. Soc.* **102**, 939 (1980)] which lacks the d polarization functions on each center. In the volume of interest, the maximum relative difference between the 6-31g* and 3-21g potentials was smaller than 5%. That means that further refinement of the basis set will not significantly change the quality of the present results.
- [16] A. A. Odintsov, *Phys. Rev. Lett.* **85**, 150 (2000).
- [17] We checked that the discreteness of the electronic spectrum had no spurious effect on the response of the system by varying the tube length and by modifying the smearing factor used in the numerical convergence study.
- [18] S. Luryi, *Appl. Phys. Lett.* **52**, 501 (1988).
- [19] J. D. Jackson, *Classical Electrodynamics* (John Wiley, New York, 1998).
- [20] Equations (1)–(3) reduce to the expected limiting behavior for the conductive cylinder for $\epsilon \rightarrow \infty$ (dielectric metallization limit) and $k_s \rightarrow \infty$ (surface state metallization limit), for the dielectric cylinder for $k_s \rightarrow 0$ (dielectric cylinder limit) and point charge solution for $k_s \rightarrow 0$, $\epsilon \rightarrow 1$ limit (free-space limit).
- [21] S. V. Kalinin, V. Meunier, J. Shin, A. P. Baddorf, C. Staii, and A. T. Johnson (to be published).